The Astrophysical Journal, 792:78 (7pp), 2014 September 1 doi:10.1088/0004-637X/792/1/78
© 2014. The American Astronomical Society. All rights reserved. Printed in the U.S.A.

THE FORMATION OF MASSIVE PRIMORDIAL STARS IN THE PRESENCE OF MODERATE UV BACKGROUNDS

M. A. Latif[1], D. R. G. Schleicher[1], S. Bovino[1], T. Grassi[2,3], and M. Spaans[4]
[1] Institut für Astrophysik, Georg-August-Universität, Friedrich-Hund-Platz 1, D-37077 Göttingen, Germany; mlatif@astro.physik.uni-goettingen.de
[2] Centre for Star and Planet Formation, Natural History Museum of Denmark, Øster Voldgade 5-7, DK-1350 Copenhagen, Denmark
[3] Niels Bohr Institute, University of Copenhagen, Juliane Maries Vej 30, DK-2100 Copenhagen, Denmark
[4] Kapteyn Astronomical Institute, University of Groningen, 9700-AV Groningen, The Netherlands
Received 2014 June 5; accepted 2014 July 15; published 2014 August 18

ABSTRACT

Radiative feedback produced by stellar populations played a vital role in early structure formation. In particular, photons below the Lyman limit can escape the star-forming regions and produce a background ultraviolet (UV) flux, which consequently may influence the pristine halos far away from the radiation sources. These photons can quench the formation of molecular hydrogen by photodetachment of H^-. In this study, we explore the impact of such UV radiation on fragmentation in massive primordial halos of a few times $10^7\ M_\odot$. To accomplish this goal, we perform high resolution cosmological simulations for two distinct halos and vary the strength of the impinging background UV field in units of J_{21} assuming a blackbody radiation spectrum with a characteristic temperature of $T_{\rm rad} = 10^4$ K. We further make use of sink particles to follow the evolution for 10,000 yr after reaching the maximum refinement level. No vigorous fragmentation is observed in UV-illuminated halos while the accretion rate changes according to the thermal properties. Our findings show that a few 10^2–10^4 solar mass protostars are formed when halos are irradiated by $J_{21} = 10$–500 at $z > 10$ and suggest a strong relation between the strength of the UV flux and mass of a protostar. This mode of star formation is quite different from minihalos, as higher accretion rates of about 0.01–0.1 $M_\odot$ yr^{-1} are observed by the end of our simulations. The resulting massive stars are potential cradles for the formation of intermediate-mass black holes at earlier cosmic times and contribute to the formation of a global X-ray background.

Key words: cosmology: theory – early universe – galaxies: formation – methods: numerical

Online-only material: color figures

1. INTRODUCTION

The first generation of stars, the so-called Population III (Pop III) stars, ushered the universe out of the cosmic dark ages and brought the first light in the cosmos. They are presumed to be assembled in dark matter halos of 10^5–$10^6\ M_\odot$ at $z = 20$–30 (Abel et al. 2002; Johnson & Khochfar 2011; Clark et al. 2011; Greif et al. 2012; Stacy et al. 2012; Latif et al. 2013c; Bovino et al. 2014; Susa et al. 2014) and influenced the subsequent structure formation via mechanical, chemical and radiative feedback (Ciardi & Ferrara 2005; Schleicher et al. 2008; Latif et al. 2012; Maio et al. 2011). Pop III stars enriched the intergalactic medium with metals and led to the second generation of stars known as Population II (Pop II) stars. According to the hierarchical paradigm of structure formation, the first galaxies are formed in massive primordial halos of 10^7–$10^8\ M_\odot$ at about $z = 15$ most likely hosting both stellar populations (Greif et al. 2008; Wise et al. 2008; Bromm et al. 2009; Latif et al. 2011a).

During the epoch of reionization, radiation emitted by the stellar population not only photo-ionized the gas but also photo-dissociated H_2 and HD molecules. Molecular hydrogen is the main coolant in primordial gas, which can bring the gas temperature down to a few hundred Kelvin and may induce star formation. In the presence of an intense ultraviolet (UV) flux, the formation of H_2 remains suppressed (due to photodetachment of H^-, which is the main pathway of H_2 formation) in pristine halos. Under these conditions, cooling only proceeds via Lyα radiation in massive primordial halos of 10^7–$10^8\ M_\odot$ and massive objects are expected to form and are known as direct collapse black holes (DCBHs; Oh & Haiman 2002; Spaans & Silk 2006; Begelman et al. 2006; Lodato & Natarajan 2006; Volonteri 2010; Schleicher et al. 2010; Latif et al. 2011b, 2013a, 2013e, 2014b; Johnson et al. 2011; Volonteri & Bellovary 2012; Haiman 2013; Prieto et al. 2013; Whalen et al. 2013b; Aykutalp et al. 2013; Yue et al. 2014; Inayoshi et al. 2014; Visbal et al. 2014).

The formation of DCBHs requires a critical strength of UV flux above which halos remain H_2 free (Omukai 2001; Shang et al. 2010; Latif et al. 2014a; Johnson et al. 2014). Such a UV flux can only exist in the close vicinity of star-forming galaxies (Dijkstra et al. 2008, 2014; Agarwal et al. 2012, 2014) and the mass scales of the resulting stars have been explored in recent studies. In fact, high resolution numerical simulations show that supermassive stars of $\sim 10^5\ M_\odot$ form in the presence of strong UV flux (Bromm & Loeb 2003; Wise et al. 2008; Regan & Haehnelt 2009; Latif et al. 2011b, 2013a, 2013b, 2013d, 2013e; Regan et al. 2014) and agree with theoretical predictions (Begelman et al. 2008; Begelman 2010; Ball et al. 2011, 2012; Hosokawa et al. 2012, 2013; Schleicher et al. 2013; Whalen et al. 2013a). Employing a cosmological framework following the formation and accretion of the resulting supermassive objects, Ferrara et al. (2014) derived detailed predictions of the mass function of the first high-mass black holes.

On the other hand, moderate strengths of the background UV flux may occur more often during the epoch of reionization without requiring the presence of nearby sources. In the ubiquity of such moderate UV fluxes, formation of H_2 does occur and may lead to star formation. Particularly, during the epoch of reionization the dominant background flux is emitted by Pop II stars. The strength of such UV flux to dissociate H_2 formation was quantified in a recent study by Latif et al. (2014a), who

Table 1
Properties of the Simulated Halos for J_{21}

Model No	J_{21} in Units of J_{21}	Mass ($M_\odot$)	Redshift z	Spin Parameter λ	Sink Particle Masses ($M_\odot$)
A				0.034	
	10	4.3×10^7	10.98		1461, 231
	100	5.45×10^7	10.63		7337
	500	5.47×10^7	10.60		22739
B				0.03	
	10	2.9×10^7	11.73		623
	100	3.2×10^7	11.38		2592
	500	3.2×10^7	11.20		24785

found that $J_{21}^{\rm crit}$ ranges from 400 to 700, higher than previous estimates. Therefore, halos exposed to fluxes below $J_{21}^{\rm crit}$ are expected to be more abundant; for $J_{21} = 10$ the fraction of halos is seven orders of magnitude higher compared to the $J_{21} = 500$ (see Figure C1 of Dijkstra et al. 2014). Thus, it is desirable to explore the typical mass scales of stars forming in halos illuminated by moderate UV fluxes emitted by Pop II stars. Safranek-Shrader et al. (2012) performed three-dimensional simulations to study the fragmentation in massive halos irradiated by Lyman–Werner flux of strength $J_{21} = 100$ for $T_{\rm rad} = 10^5$ K and found that a dense turbulent core of $10^4\ M_\odot$ forms in the center of the halo.

In this study, we explore the mass scales of stars formed under moderate strengths of the background UV flux with $T_{\rm rad} = 10^4$ K. To achieve this goal, we perform three-dimensional cosmological simulations for two halos of a few times $10^7\ M_\odot$ and vary the strength of the UV flux (hereafter called J_{21}, i.e., UV flux with energy below 13.6 eV). We employed a Jeans resolution of 32 cells during the course of the simulations and make use of sink particles to follow the evolution for 10^4 yr after reaching the maximum refinement level in the simulations. The main objective of this work is to determine the mass scale of resulting objects for a moderate UV radiation field. This has potential implications for the formation of intermediate-mass black holes in stellar clusters at earlier cosmic times. We note that the expected ionizing UV feedback from these protostars is still weak for accretion rates higher than $0.1\ M_\odot\ {\rm yr}^{-1}$ (Schleicher et al. 2013; Hosokawa et al. 2013) and is therefore neglected here.

The outline of this article is as follows. In Section 2, we describe our numerical methodology and give a brief overview of chemical network. We present our main results in Section 3 and our conclusions in Section 4.

2. COMPUTATIONAL METHODS

We employed the open source code ENZO[5] to perform three-dimensional cosmological simulations following the collapse in massive primordial halos (Bryan et al. 2014). ENZO is an adaptive mesh refinement, parallel, Eulerian code. It makes use of the piece-wise parabolic method to solve the hydrodynamical equations. The dark matter dynamics is solved by using the particle-mesh technique.

Our simulations are started with cosmological initial conditions at $z = 100$. We first run simulations with a uniform grid resolution of 128^3 cells and select the most massive dark matter halos in a computational domain with comoving size of 1 Mpc h^{-1}. The simulations are commenced with two additional nested refinement levels each with a resolution of 128^3 cells in addition to a top grid resolution of 128^3 cells and are centered on the most massive halo. We employed 5,767,168 particles to solve the dark matter dynamics. To follow the collapse of the halo additional 18 levels of refinement are applied during the course of simulations with a fixed Jeans resolution of 32 cells. We further make use of sink particles to follow the accretion for 10,000 yr after the formation of the first sink. Detailed discussions about the sink particles and the simulation setup can be found in our previous studies (Latif et al. 2013a, 2013b, 2013e, 2014c).

To follow the evolution of chemical species, the rate equations of the following species H, H^+, He, He^+, He^{++}, e^-, H^-, H_2, H_2^+ are solved in our cosmological simulations. We used the publicly available KROME package[6] (Grassi et al. 2014) to compute the evolution of chemical and thermal processes. The chemical network and the microphysics employed here are the same as in Latif et al. (2014a) including the photodetachment of H^- as well as absorption of Lyman–Werner photons. We employed the H_2 self-shielding function from Wolcott-Green et al. (2011). As shown by Shang et al. (2010) including the effect of self-shielding raises $J_{21}^{\rm crit}$ by a factor of 2–3. We have not included HD chemistry in our simulation as HD is a very fragile molecule and even weaker flux such as $J_{21} = 0.1$ is found to be sufficient to dissociate it. The same was observed in simulations of Safranek-Shrader et al. (2012).

In this study, simulations are performed for two distinct halos by varying the strength of the UV flux below the Lyman limit with $T_{\rm rad} = 10^4$ K. The properties of the simulated halos and the strength of the UV flux in units of J_{21} are listed in Table 1.

3. MAIN RESULTS

In total, we performed six cosmological simulations for two different halos of a few times $10^7\ M_\odot$ and varied the strength of J_{21} (i.e., 10, 100, and 500). We further employed sink particles, which represent the protostars in our simulations. Our results show that initially the gas is heated up to 10^4 K in the presence of the background UV flux and then cools by Lyα cooling. Depending on the strength of the UV flux, H_2 formation takes place and cooling due to the molecular hydrogen becomes effective. For $J_{21} = 10$, 100, the central temperature in the halo is about 1000 K while for $J_{21} = 500$ the temperature in the core is a few thousand Kelvin as shown in Figure 1. It is also found that for a weaker flux (i.e., $J_{21} = 10$), H_2 cooling kicks in at densities around 10^{-23} g cm^{-3} while for $J_{21} = 100$ it

[5] http://enzo-project.org/, changeset:48de94f882d8

[6] Webpage KROME: www.kromepackage.org

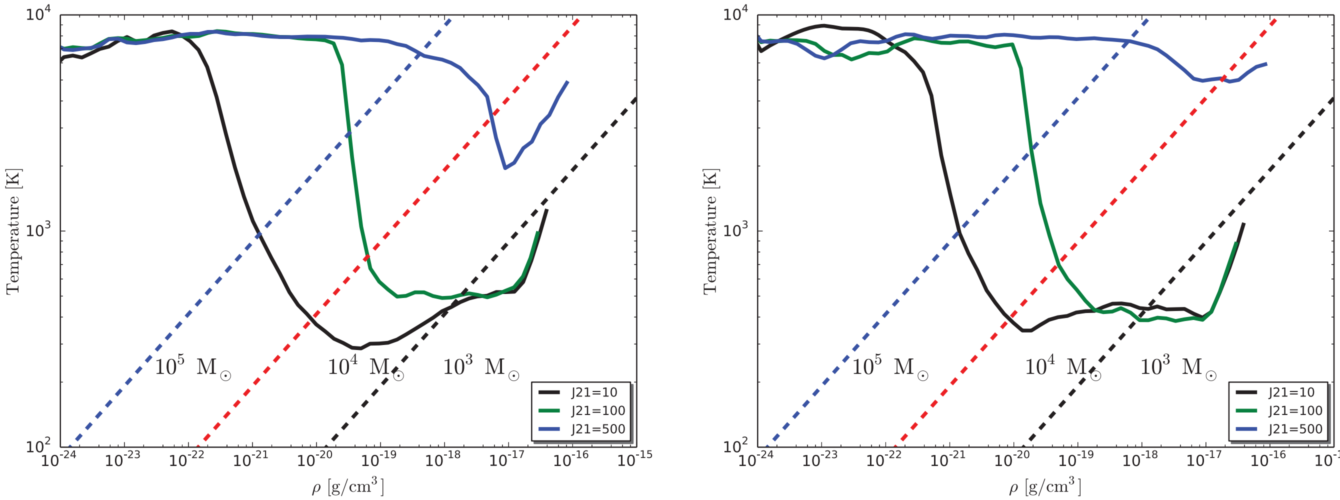

Figure 1. Average values of the temperature are plotted against density at the end point of our simulations for various strengths of J_{21}. The left panel shows halo A and the right panel stands for halo B. The dashed lines show the expected thermal Jeans mass at these scales.

(A color version of this figure is available in the online journal.)

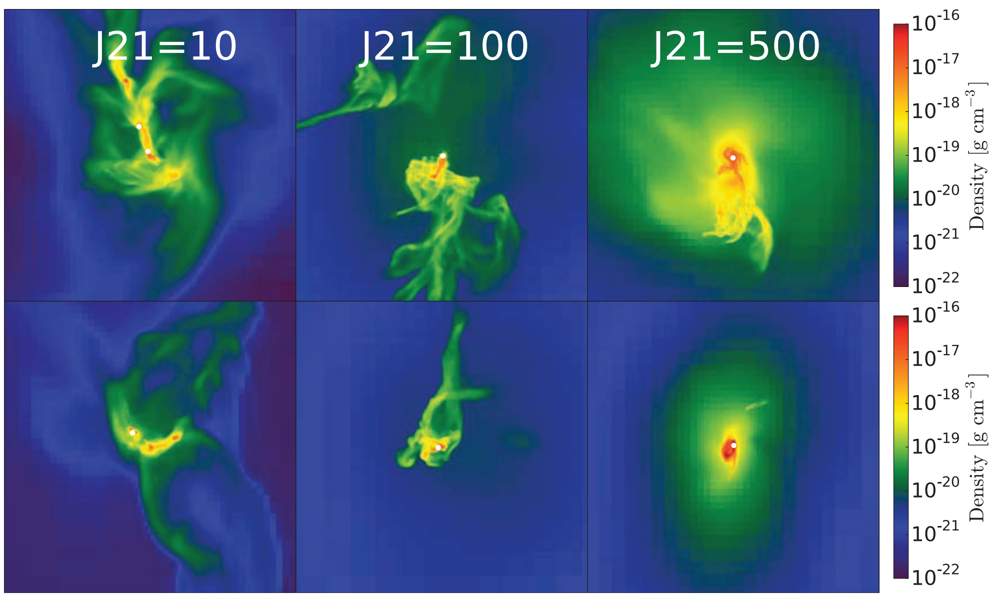

Figure 2. Final state of our simulation is represented by the average density along the line of sight for different radiation backgrounds. The top panel represents halo A and the bottom panel halo B. The overplotted white points depict sink particles. The masses of the sink particles are listed in Table 1.

(A color version of this figure is available in the online journal.)

becomes effective around 10^{-20} g cm^{-3}. For the strongest flux, it starts at even higher densities of about 10^{-18} g cm^{-3}.

The density structure for various strengths of the UV field is shown in Figure 2. It can be seen that for $J_{21} = 10$ the gas in the halos becomes clumpier and forms multiple sinks. These sinks reside inside the clumps formed by H_2 cooling, which lowers the gas temperature down to a few hundred Kelvin as shown in Figures 3 and 4. For higher values of J_{21}, the halos have less structure and the number of the sinks is reduced. This is due to the fact that the overall temperature in the halo is higher particularly in the outskirts which suppresses fragmentation. Similarly, the fraction of molecular hydrogen is significantly reduced in the surrounding of the halo. There are a few clumps with no sinks which are gravitationally unbound and have masses of the order of a few solar masses. For the strongest flux ($J_{21} = 500$), there is no sign of fragmentation as the central temperature in the halos is a few thousand Kelvin and one halo later approaches an isothermal state due to the temperature dependence of the H_2 collisional dissociation rate (Martin et al. 1996). The fraction of molecular hydrogen is significantly lower and is limited to only the core of the halos.

To further quantify the masses of the sinks formed in our simulated halos, we followed the evolution for many free-fall times. The masses of the sinks are listed in Table 1. It is found that for $J_{21} = 10$, the masses of the sinks are a few hundred to about 1500 $M_\odot$. In halo A two sinks are formed. For $J_{21} = 100$, only one massive sink is formed in each halo and their masses are 7400 and 2500 $M_\odot$. The masses of the sinks are above 22,000 solar masses for the strongest flux case and a single sink is formed per halo. Overall, our results suggest that fragmentation in the halos is reduced by increasing the strength of background UV flux according to theoretical expectations. For $J_{21} = 10$ and 100, although the central temperatures are quite similar the masses are higher by a factor of a few for $J_{21} = 100$.

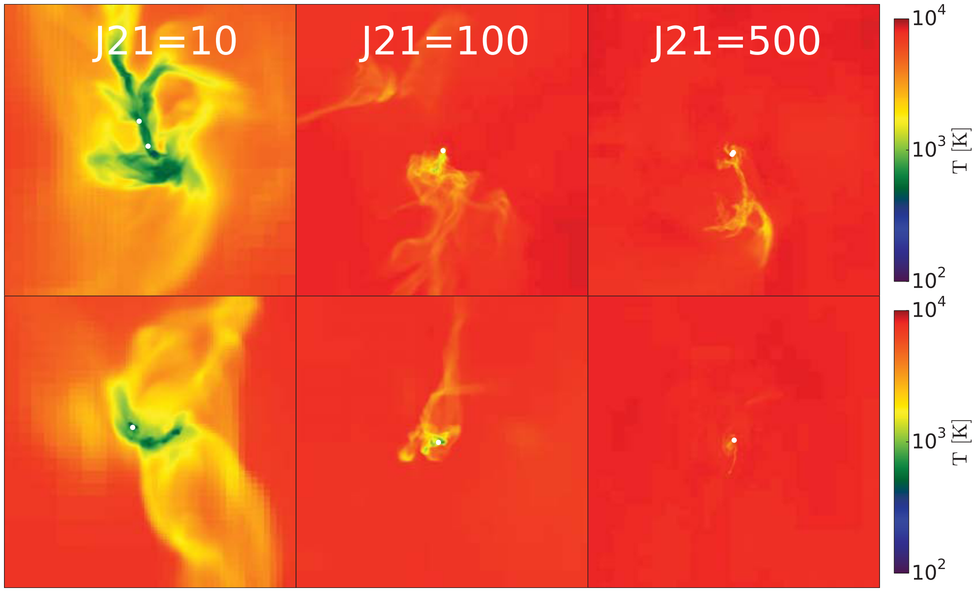

Figure 3. Temperature is shown here corresponding to the Figure 4.
(A color version of this figure is available in the online journal.)

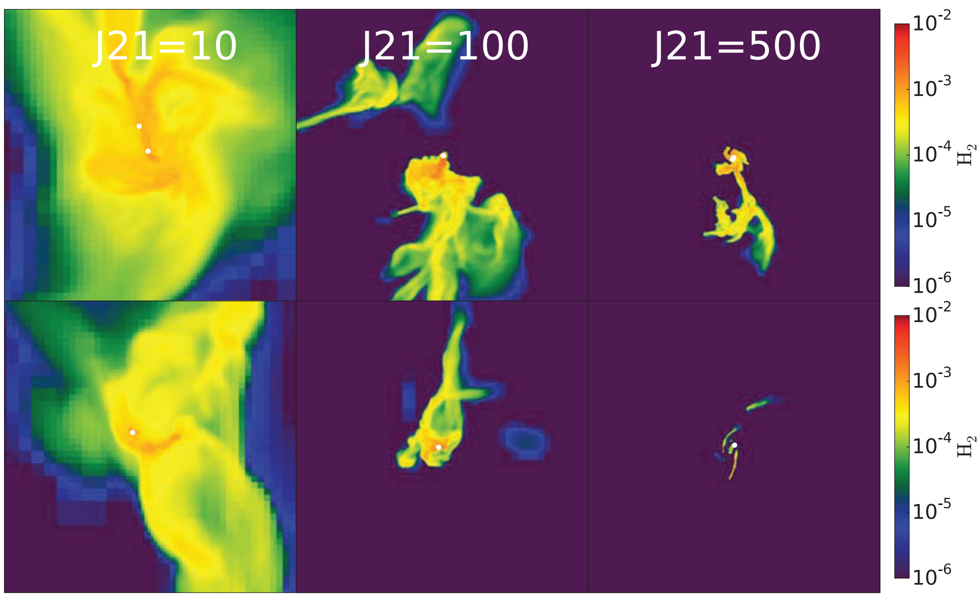

Figure 4. Abundance of molecular hydrogen is depicted here same as Figure 4.
(A color version of this figure is available in the online journal.)

This is because of the warmer gas in the surroundings of the halo, which leads to higher accretion rates and consequently higher sink masses at the end of our simulations. It is found that the masses of the sinks in halo B are about a factor of two lower compared to halo A. Overall, the average density in halo B is lower and has a higher rotational support. This leads to lower accretion rates in halo B and consequently lower sink masses.

The physical properties of the halos are depicted in Figures 5 and 6. The maximum density in the halos is $10^{-16}\,\mathrm{g\,cm^{-3}}$. The density profile follow an R^{-2} behavior at larger radii for almost all fluxes and becomes flat in the core of the halo corresponding to the Jeans length. The deviations from this behavior are observed for weaker values of J_{21} due to the additional substructure inside the halo. The difference between weaker and stronger fluxes is more prominent in halo B as it collapses almost isothermally for $J_{21} = 500$. The overall density in halo B is lower by a factor of a few compared to the halo A around 10 pc. For $J_{21} = 10$, cooling due to H_2 becomes effective in the central 10 pc of the halo. On the other hand for $J_{21} = 100$ it is limited to the central parsec of the halo while for $J_{21} = 500$ cooling due to the molecular hydrogen is not very effective due to its lower abundance.

The impact of different thermal evolutions is also reflected in the infall velocities of the halos. Higher temperatures lead to higher infall velocities and also indicate lower molecular hydrogen fractions in those halos. Similarly lower infall velocities are observed for the weaker fluxes indicating that the halo is in the molecular cooling phase. Halo B has lower radial infall velocities compared to halo A. It is further found that the accretion rates are slightly higher for stronger fluxes and are lower in halo B compared to halo A. The decline in accretion rates toward the center is due to the increasing pressure support within the Jeans

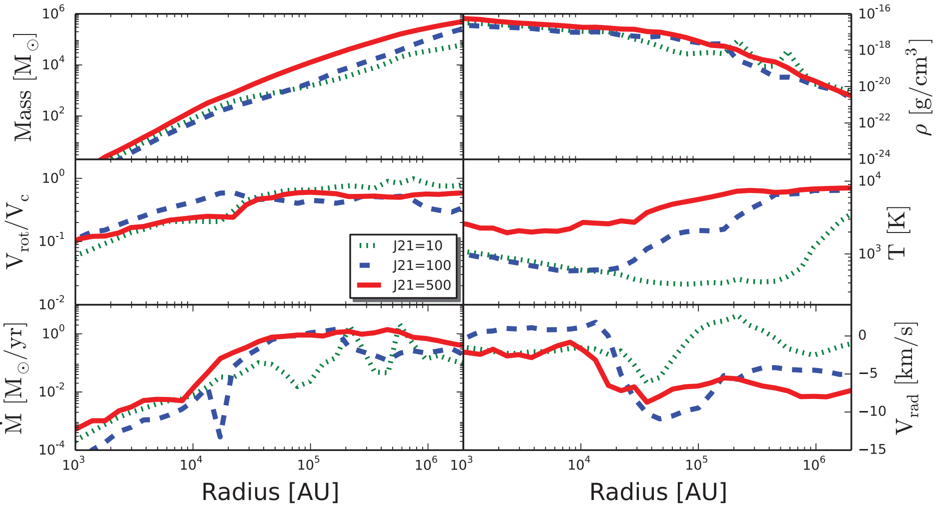

Figure 5. Radially averaged spherically binned profiles are shown here for halo A at the end point of our simulations. Each line style represents a different strength of the UV flux as shown in the legend. The top panels show the mass and density, the middle panels show the ratio $v_{\rm rot}/v_c$ and the temperature, and the bottom panels show the mass accretion rates and infall velocities.

(A color version of this figure is available in the online journal.)

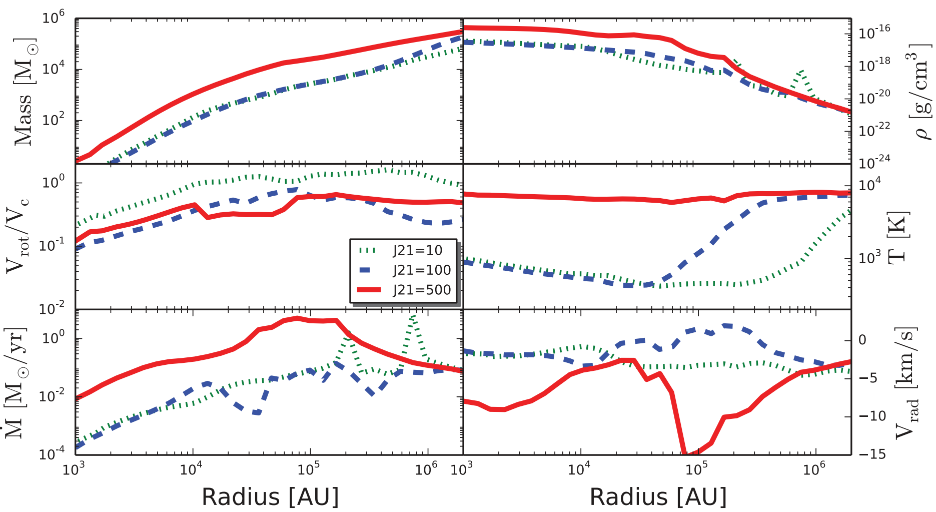

Figure 6. Same as Figure 5 but for halo B.

(A color version of this figure is available in the online journal.)

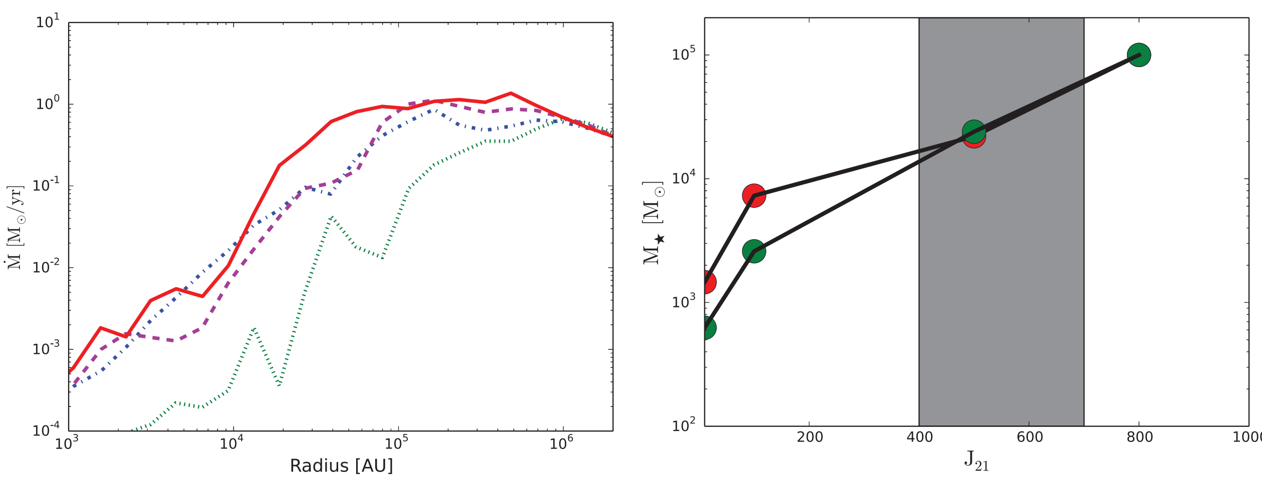

Figure 7. Left panel shows the time evolution of the mass accretion rates against radius for $J_{21} = 500$. The green line shows the mass accretion rates at the formation time of the sink while the red line depicts the evolution for 10,000 yr. The blue and magenta lines represent the time evolution of 5000 and 8000 yr after the formation of sink. The right panel shows the masses of protostars/sinks for various strengths of J_{21}. The dashed vertical shaded region represents the range of critical values, i.e., $J_{21} = 400$–700. The red and blue circles represent halos A and B, respectively. The last two data points are taken from Latif et al. (2013e) and indicate the expected masses for $J_{21} > J_{21}^{\rm crit}$.

(A color version of this figure is available in the online journal.)

length. The accretion rates in halo A range from $\sim 1\ M_\odot\ \mathrm{yr}^{-1}$ for $J_{21} = 500$ to $\sim 0.1\ M_\odot\ \mathrm{yr}^{-1}$ for $J_{21} = 10$. The intermediate case with $J_{21} = 100$ still has an accretion rate close to $\sim 1\ M_\odot\ \mathrm{yr}^{-1}$ on scales of 10^5 AU, but decreases to $\sim 0.1\ M_\odot\ \mathrm{yr}^{-1}$ on larger scales, indicating that the central mass will increase more slowly at later times. For halo B, the accretion rates are reduced by roughly a factor of three on large scales, and also the intermediate case is closer to $\sim 0.1\ M_\odot\ \mathrm{yr}^{-1}$. The enclosed mass in the halos is higher for stronger fluxes. This is due to the higher infall velocities and higher accretion rates for these cases. It is also found that halo B has higher rotational support. We further noted that the accretions rates increased during the course of simulations and are shown for a representative case in Figure 7.

We show the masses of the sink particles for various values of J_{21} in Figure 7. In the presence of UV feedback, they are very massive typically above one thousand solar masses. This figure shows an increase in the mass of sinks with the strength of the UV flux, i.e., the higher the UV flux the more massive the sink. Fragmentation may occur at larger scales but may not be able to prevent the formation of massive stars. We expect that these massive to supermassive stars are potential candidates for progenitors of intermediate to supermassive black holes.

4. DISCUSSION AND CONCLUSIONS

In this article, we explored fragmentation in massive primordial halos of a few times $10^7\ M_\odot$ irradiated by different UV fluxes below the Lyman limit. To achieve this goal, we performed high resolution cosmological simulations for two distinct halos collapsing at $z > 10$ and varied the strength of the UV flux from 10 to 500 in units of J_{21}. We exploited the adaptive mesh refinement technique to follow the collapse of the halo by employing additional 18 dynamical refinement levels during the course of simulations which yields an effective resolution of about 100 AU. To further follow the evolution for longer timescales, sink particles representing protostars were employed. A fixed Jeans resolution of 32 cells were mandated during the entire course of simulations.

Our findings show that the formation of H_2 gets delayed and no strong fragmentation occurs in the halos illuminated by the UV flux of 10–500 J_{21}. For $J_{21} = 10$, in our simulated halos binary or multiple systems may likely form but for higher values of J_{21} only one single object is formed. At the end of our simulations, massive sink particles of a few 10^2–10^4 solar masses are formed and large accretion rates of about 0.1–0.01 $M_\odot\ \mathrm{yr}^{-1}$ are observed. The relatively high accretion rates distinguish them from normal star formation mode in minihalos.

H_2 cooling reaches local thermal equilibrium at densities higher than $10^4\ \mathrm{cm}^{-3}$ and the cooling rate scales as density while compressional heating varies with $\rho^{3/2}$. So the expected polytropic index stiffens (i.e., $\gamma > 1$) and suppresses fragmentation (Spaans & Silk 2000). Of course, the possibility of fragmentation at higher density cannot be completely ruled out and low mass stars may form in addition to the most massive object. However, it is very likely that the formation of massive stars will be the outcome. Such massive stars formed are also potential candidates for progenitors of intermediate-mass black holes.

Safranek-Shrader et al. (2012) performed similar simulations for a halo of similar mass irradiated by the background UV flux emitted by Pop III stars. They also found that the gas self-shields from the UV flux and a dense core of $10^4\ M_\odot$ develops. They further used sink particles to follow the simulations for longer times and found that a massive sink of about 1000 solar masses is formed. Their study is comparable to $J_{21} = 10$ in our simulations due to the background UV flux emitted by two different stellar populations. They have employed a radiation spectrum with $T_{\mathrm{rad}} = 10^5$ K in their calculations which mainly dissociates the molecular hydrogen via the Solomon process and H_2 self-shielding is more important in contrast to our study.

In particular, we compare the accretion rates at the same times in both simulations and our results appear rather consistent. We note however that there is no one-to-one correspondence, as the thermal evolution does not precisely match and our halo is somewhat warmer on larger scales. In addition, there are of course fluctuations from halo to halo, so some variation between the halos is expected, as we also see here when comparing halos A and B.

It may also be noted that ignoring the effect of H_2 self-shielding decreases the value of J_{21}^{crit} by a factor of 2–3 (Shang et al. 2010) which may consequently influence the resulting masses of protostars. In this case, the masses of the stars for a given strength of J_{21} are expected to be higher by about an order of magnitude due to the higher accretion rates. We here consider an approximate treatment for the computation of column densities of H_2. In the future a ray-tracing algorithm should be employed to more precisely compute the column densities and the directional dependence of the radiation source should be taken into account.

To further explore the possible fragmentation at higher densities, we in total added 27 refinement levels which yield resolutions down to sub-AU scales (0.25 AU) and peak densities of $10^{-11}\ \mathrm{g\ cm}^{-3}$. We however do not see any indication of further fragmentation for these runs. Such verification further confirms that even if fragmentation occurs at later stages the mass of the central object would not change significantly. Our results for $J_{21} = 10$ are in agreement with Hirano et al. (2014) who simulated about 100 minihalos and found that even massive stars of a thousand solar masses can form in the presence of similar mass accretion rates found in this study.

We stopped our simulations 10,000 yr after the formation of the sink due to computational constraints. We also note that our simulations do not include ionizing UV feedback from the protostar. As long as the accretion rates remain higher than $0.1\ M_\odot\ \mathrm{yr}^{-1}$, no strong feedback is expected (Hosokawa et al. 2012, 2013; Schleicher et al. 2013). We note that some of the accretion rates in our simulations, especially for $J_{21} = 10$, are already close to the threshold of $0.1\ M_\odot\ \mathrm{yr}^{-1}$. In halo B, even the case with $J_{21} = 100$ shows a similar behavior. In halo A, such a decrease may occur at later times for the same radiation background, and is currently reflected in a lower accretion rate on larger scales. For $J_{21} = 500$, on the other hand, the accretion rates are significantly above the threshold for both halos, so we expect the accretion to continue for significantly longer times. Overall, the accretion seems likely to stop earlier for lower values of J_{21} as a result of ionizing feedback. These cases may thus be already close to the final stellar masses, while significant accretion may still occur for higher values of J_{21}.

We also assumed that halos are metal-free and given the patchy distribution of the metal, such halos may exist down to $z = 6$ (Trenti et al. 2009). However, if metal enrichment takes places in these halos it will lead to fragmentation and most likely a star cluster of low-mass stars (Safranek-Shrader et al. 2014; Peters et al. 2014). Even a small amount of dust, i.e., $10^{-5}\,Z/Z_\odot$, is sufficient to boost the H_2 fraction and induce fragmentation

(Cazaux & Spaans 2009). In fact, recent observations suggest the potential presence of intermediate-mass black holes in globular clusters (Kamann et al. 2014).

From the results given here, we deduce that massive to supermassive stars may be more common than previously expected, and can also form for radiative backgrounds $J_{21} < J_{21}^{\rm crit}$. Based on the recent estimates of Dijkstra et al. (2014) for the expected density of halos for various UV field strengths, the expected fraction of halos exposed to $J_{21} < J_{21}^{\rm crit}$ is a few orders of magnitude higher. We expect such stars to produce a considerable amount of UV feedback once they are on the main sequence, thus considerably contributing to the ionization of their environment, and perhaps also to the epoch of reionization. At the end of their lives, they may collapse to an intermediate-mass black hole, and the X-rays released during their formation may contribute to the establishment of a global background (Yue et al. 2013).

The simulations described in this work were performed using the Enzo code, developed by the Laboratory for Computational Astrophysics at the University of California in San Diego (http://lca.ucsd.edu). We acknowledge research funding by Deutsche Forschungsgemeinschaft (DFG) under grant SFB 963/1 (project A12) and computing time from HLRN under project nip00029. D.R.G.S. and S.B. thank the DFG for funding via the Schwerpunktprogram SPP 1573 "Physics of the Interstellar Medium" (grant SCHL 1964/1 − 1). T.G. acknowledges the Centre for Star and Planet Formation funded by the Danish National Research Foundation. The simulation results are analyzed using the visualization toolkit for astrophysical data YT (Turk et al. 2011).

REFERENCES

Abel, T., Bryan, G. L., & Norman, M. L. 2002, Sci, 295, 93
Agarwal, B., Dalla Vecchia, C., Johnson, J. L., Khochfar, S., & Paardekooper, J.-P. 2014, MNRAS, 443, 648
Agarwal, B., Khochfar, S., Johnson, J. L., et al. 2012, MNRAS, 425, 2854
Aykutalp, A., Wise, J. H., Meijerink, R., & Spaans, M. 2013, ApJ, 771, 50
Ball, W. H., Tout, C. A., & Żytkow, A. N. 2012, MNRAS, 421, 2713
Ball, W. H., Tout, C. A., Żytkow, A. N., & Eldridge, J. J. 2011, MNRAS, 414, 2751
Begelman, M. C. 2010, MNRAS, 402, 673
Begelman, M. C., Rossi, E. M., & Armitage, P. J. 2008, MNRAS, 387, 1649
Begelman, M. C., Volonteri, M., & Rees, M. J. 2006, MNRAS, 370, 289
Bovino, S., Latif, M. A., Grassi, T., & Schleicher, D. R. G. 2014, MNRAS, 441, 2181
Bromm, V., & Loeb, A. 2003, ApJ, 596, 34
Bromm, V., Yoshida, N., Hernquist, L., & McKee, C. F. 2009, Natur, 459, 49
Bryan, G. L., Norman, M. L., O'Shea, B. W., et al. 2014, ApJS, 211, 19
Cazaux, S., & Spaans, M. 2009, A&A, 496, 365
Ciardi, B., & Ferrara, A. 2005, SSRv, 116, 625
Clark, P. C., Glover, S. C. O., Smith, R. J., et al. 2011, Sci, 331, 1040
Dijkstra, M., Ferrara, A., & Mesinger, A. 2014, MNRAS, 442, 2036
Dijkstra, M., Haiman, Z., Mesinger, A., & Wyithe, J. S. B. 2008, MNRAS, 391, 1961
Ferrara, A., Salvadori, S., Yue, B., & Schleicher, D. R. G. 2014, MNRAS, 443, 2410
Grassi, T., Bovino, S., Schleicher, D. R. G., et al. 2014, MNRAS, 439, 2386
Greif, T. H., Bromm, V., Clark, P. C., et al. 2012, MNRAS, 424, 399
Greif, T. H., Johnson, J. L., Klessen, R. S., & Bromm, V. 2008, MNRAS, 387, 1021
Haiman, Z. 2013, The First Galaxies (Astrophysics and Space Science Library, Vol. 396; Berlin: Springer), 293
Hirano, S., Hosokawa, T., Yoshida, N., et al. 2014, ApJ, 781, 60
Hosokawa, T., Omukai, K., & Yorke, H. W. 2012, ApJ, 756, 93
Hosokawa, T., Yorke, H. W., Inayoshi, K., Omukai, K., & Yoshida, N. 2013, ApJ, 778, 178
Inayoshi, K., Omukai, K., & Tasker, E. J. 2014, arXiv:1404.4630
Johnson, J. L., & Khochfar, S. 2011, MNRAS, 413, 1184
Johnson, J. L., Khochfar, S., Greif, T. H., & Durier, F. 2011, MNRAS, 410, 919
Johnson, J. L., Whalen, D. J., Agarwal, B., Paardekooper, J.-P., & Khochfar, S. 2014, arXiv:1405.2081
Kamann, S., Wisotzki, L., Roth, M. M., et al. 2014, A&A, 566, A58
Latif, M. A., Bovino, S., Van Borm, C., et al. 2014a, MNRAS, 443, 1979
Latif, M. A., Niemeyer, J. C., & Schleicher, D. R. G. 2014b, MNRAS, 440, 2969
Latif, M. A., Schleicher, D. R. G., & Schmidt, W. 2014c, MNRAS, 440, 1551
Latif, M. A., Schleicher, D. R. G., Schmidt, W., & Niemeyer, J. 2013a, MNRAS, 433, 1607
Latif, M. A., Schleicher, D. R. G., Schmidt, W., & Niemeyer, J. 2013b, MNRAS, 430, 588
Latif, M. A., Schleicher, D. R. G., Schmidt, W., & Niemeyer, J. 2013c, ApJL, 772, L3
Latif, M. A., Schleicher, D. R. G., Schmidt, W., & Niemeyer, J. 2013d, MNRAS, 432, 668
Latif, M. A., Schleicher, D. R. G., Schmidt, W., & Niemeyer, J. C. 2013e, MNRAS, 436, 2989
Latif, M. A., Schleicher, D. R. G., & Spaans, M. 2012, A&A, 540, A101
Latif, M. A., Schleicher, D. R. G., Spaans, M., & Zaroubi, S. 2011a, A&A, 532, A66
Latif, M. A., Zaroubi, S., & Spaans, M. 2011b, MNRAS, 411, 1659
Lodato, G., & Natarajan, P. 2006, MNRAS, 371, 1813
Maio, U., Khochfar, S., Johnson, J. L., & Ciardi, B. 2011, MNRAS, 414, 1145
Martin, P. G., Schwarz, D. H., & Mandy, M. E. 1996, ApJ, 461, 265
Oh, S. P., & Haiman, Z. 2002, ApJ, 569, 558
Omukai, K. 2001, ApJ, 546, 635
Peters, T., Schleicher, D. R. G., Smith, R. J., Schmidt, W., & Klessen, R. S. 2014, MNRAS, 442, 3112
Prieto, J., Jimenez, R., & Haiman, Z. 2013, MNRAS, 436, 2301
Regan, J. A., & Haehnelt, M. G. 2009, MNRAS, 393, 858
Regan, J. A., Johansson, P. H., & Haehnelt, M. G. 2014, MNRAS, 439, 1160
Safranek-Shrader, C., Agarwal, M., Federrath, C., et al. 2012, MNRAS, 426, 1159
Safranek-Shrader, C., Milosavljević, M., & Bromm, V. 2014, MNRAS, 440, L76
Schleicher, D. R. G., Galli, D., Palla, F., et al. 2008, A&A, 490, 521
Schleicher, D. R. G., Palla, F., Ferrara, A., Galli, D., & Latif, M. 2013, A&A, 558, A59
Schleicher, D. R. G., Spaans, M., & Glover, S. C. O. 2010, ApJL, 712, L69
Shang, C., Bryan, G. L., & Haiman, Z. 2010, MNRAS, 402, 1249
Spaans, M., & Silk, J. 2000, ApJ, 538, 115
Spaans, M., & Silk, J. 2006, ApJ, 652, 902
Stacy, A., Greif, T. H., & Bromm, V. 2012, MNRAS, 422, 290
Susa, H., Hasegawa, K., & Tominaga, N. 2014, arXiv:1407.1374
Trenti, M., Stiavelli, M., & Michael Shull, J. 2009, ApJ, 700, 1672
Turk, M. J., Smith, B. D., Oishi, J. S., et al. 2011, ApJS, 192, 9
Visbal, E., Haiman, Z., & Bryan, G. L. 2014, MNRAS, 442, L100
Volonteri, M. 2010, A&ARv, 18, 279
Volonteri, M., & Bellovary, J. 2012, RPPh, 75, 124901
Whalen, D. J., Even, W., Lovekin, C. C., et al. 2013a, ApJ, 768, 195
Whalen, D. J., Johnson, J. L., Smidt, J., et al. 2013b, ApJ, 774, 64
Wise, J. H., Turk, M. J., & Abel, T. 2008, ApJ, 682, 745
Wolcott-Green, J., Haiman, Z., & Bryan, G. L. 2011, MNRAS, 418, 838
Yue, B., Ferrara, A., Salvaterra, R., Xu, Y., & Chen, X. 2013, MNRAS, 433, 1556
Yue, B., Ferrara, A., Salvaterra, R., Xu, Y., & Chen, X. 2014, MNRAS, 440, 1263